The MNK1/2-eIF4E axis supports immune suppression and metastasis in postpartum breast cancer

Qianyu Guo[1, 2‡], Margarita Bartish[1, 2‡], Christophe Gonçalves[2], Fan Huang[1, 2], Julian Smith-Voudouris[1,2], Sai Sakktee Krisna[2, 3, 4], Samuel E. J. Preston[1, 2], Audrey Emond[2], Vivian Z. Li[2], Claudia U. Duerr[5], Yirui Gui[2], Aurélie Cleret-Buhot[6], Pamela Thebault[6, 7, 8, 9], Hanne Lefrère[10], Liesbeth Lenaerts[10], Dany Plourde[2], Jie Su[2], Barbara C. Mindt[4, 5], Shannon A. Hewgill[4, 5], Tiziana Cotechini[11], Charles C. T. Hindmarch[12], William Yang[1], Elie Khoury[1], Yao Zhan[1], Valeria Narykina[2], Yuhong Wei[13], Giuseppe Floris[14,15], Mark Basik[1,2], Frédéric Amant[10, 16], Daniela F. Quail[3,13], Réjean Lapointe[6, 7, 8], Jörg H. Fritz[4, 5, 13], Sonia V. del Rincon*[1, 2], Wilson H. Miller Jr.*[1, 2, 17]

1 Department of Experimental Medicine, Faculty of Medicine, McGill University

2 Segal Cancer Center, Lady Davis Institute & Jewish General Hospital

3 Department of Physiology, Faculty of Medicine, McGill University

4 McGill University Research Centre on Complex Traits

5 Department of Microbiology & Immunology, Faculty of Medicine, McGill University

6 Centre de Recherche du Centre Hospitalier de l'Université de Montréal (CRCHUM)

7 Institut du cancer de Montréal

8 Département de Médecine, Faculté de Médecine, Université de Montréal

9 Clinical Immuno-Monitoring Core Facility, CRCHUM

10 Department of Oncology, Katholieke Universiteit Leuven

11 Department of Biomedical and Molecular Sciences, Queen's University

12 Queen's Cardiopulmonary Unit, Queen's University

13 Rosalind and Morris Goodman Cancer Research Centre, McGill University

14 Department of Pathology, University Hospitals Leuven

15 Department of Imaging and Pathology, Katholieke Universiteit Leuven

16 Center Gynaecologic Oncology Amsterdam at the Netherlands Cancer Institute and Amsterdam University Medical Centers

17 Montreal Rossy Cancer Network

‡ These authors contributed equally to this work

* Corresponding authors:

Wilson H. Miller Jr.: wmiller@ldi.jgh.mcgill.ca

Lady Davis Institute for Medical Research
3755 Chemin de la Côte Ste Catherine
Montréal, Québec
Canada H3T 1E2
Phone: 514-340-8260

Sonia V. del Rincón: sonia.delrincon@mcgill.ca

Lady Davis Institute for Medical Research
3755 Chemin de la Côte Ste Catherine
Montréal, Québec
Canada H3T 1E2
Phone: 514-340-8260

Running title: Pleiotropic roles of the MNK1/2-eIF4E axis in PPBC

Key words: breast cancer, mammary gland involution, metastasis, tumor microenvironment, phospho-eIF4E

Competing interests statement

The authors declare no conflicts of interest.

Abstract

Breast cancer diagnosed within 10 years following childbirth is defined as postpartum breast cancer (PPBC) and is highly metastatic. Interactions between immune cells and other stromal cells within the involuting mammary gland are fundamental in facilitating an aggressive tumor phenotype. The MNK1/2-eIF4E axis promotes translation of pro-metastatic mRNAs in tumor cells, but its role in modulating the function of non-tumor cells in the PPBC microenvironment has not been explored. Here we used a combination of in vivo PPBC models and in vitro assays to study the effects of inactivation of the MNK1/2-eIF4E axis on the pro-tumor function of select cells of the TME. PPBC mice deficient for phospho-eIF4E ($eIF4E^{S209A}$) were protected against lung metastasis and exhibited differences in the tumor and lung immune microenvironment compared to wild-type mice. Moreover, expression of fibroblast-derived IL-33, an alarmin known to induce invasion, was repressed upon MNK1/2-eIF4E axis inhibition. Imaging mass cytometry on PPBC and non-PPBC patient samples indicated that human PPBC contains phospho-eIF4E high-expressing tumor cells and $CD8^+$ T cells displaying markers of an activated dysfunctional phenotype. Finally, inhibition of MNK1/2 combined with anti-PD-1 therapy blocked lung metastasis of PPBC. These findings implicate the involvement of the MNK1/2-eIF4E axis during PPBC metastasis and suggest a promising immunomodulatory route to enhance the efficacy of immunotherapy by blocking phospho-eIF4E.

Statement of significance

This study investigates the MNK-eIF4E signaling axis in tumor and stromal cells in metastatic breast cancer and reveals that MNK1/2 inhibition suppresses metastasis and sensitizes tumors to anti-PD1 immunotherapy.

Introduction

Postpartum breast cancer (PPBC) is defined as breast cancer diagnosed within 10 years of parturition (1). Given its highly metastatic nature (1,2), the patient prognosis is poor. The physiological process of mammary gland (MG) involution, the remodeling of the breast tissue back to its pre-pregnant state, has been hypothesized to cause premalignant epithelial cells to adopt invasive properties (2). Involution, akin to the process of wound healing, is accompanied by an orchestrated immune cell infiltration into the mammary gland (3). Data from murine PPBC models suggest that interactions between innate and adaptive immune cells as well as involution-activated fibroblasts are fundamental in establishing a suppressed microenvironment that is favorable for metastatic spread.

Cancer cell invasiveness is regulated by growth factors, cytokines, and chemokines produced by tumor cells and associated stromal cells within the TME. Recently the IL-33/ST2 signaling axis has come to the forefront as an important mediator of metastasis. IL-33 is an alarmin cytokine of the IL-1 family, is involved in inflammation, tissue homeostasis and tumor progression, and signals via binding to the ST2 receptor (4). Although there are many cellular sources of IL-33, its secretion by cancer associated fibroblasts has been shown to promote the epithelial-to-mesenchymal like transition and tumor cell invasion (5,6). IL-33 can also promote tumor progression and immune suppression via activation of immune cells such as $CD11b^{+}Gr1^{+}$ myeloid-derived suppressor cells (MDSCs) (7) and innate lymphoid cells type 2 (ILC2) (8). Once activated, these cells serve as potent inhibitors of cytotoxic T cell tumor infiltration and anti-tumor function (9,10).

Regulation of gene expression at the level of mRNA translation initiation is becoming increasingly studied in the field of onco-immunology. Indeed, dysregulation of translational

control is a prominent feature of many cancers (11). For example, elevated levels of the eukaryotic translation initiator factor 4E (eIF4E), which binds to the 7-methylguanosine cap at the 5' end of the mRNA, are associated with malignancy and poor prognosis in several cancer types (12). eIF4E can be phosphorylated at serine 209 (S209) by MAP kinase-interacting serine/threonine-protein kinases 1 and 2 (MNK1/2), and this post-translational modification is essential for its pro-invasive effects (13). Increased MNK1/2 activity has been associated with therapeutic resistance, tumorigenesis, invasion and metastasis (14). We and others have previously shown that phosphorylation of eIF4E leads to the translational upregulation of mRNAs, such as *Myc*, *Mcl1*, *Mmp3* and *Snai1*, that support tumor cell survival and a pro-invasive phenotype (13,15). In the context of the tumor microenvironment (TME), phospho-eIF4E has recently been reported to reinforce the survival of pro-metastatic neutrophils (16) and regulate the pro-tumor functions of bone marrow-derived macrophages (17). In murine models of melanoma, we showed that phospho-eIF4E deficiency associates with decreased PD-L1 expression on dendritic cells and MDSCs in the TME (18). However, there remain large gaps in our understanding of how the regulation of eIF4E phosphorylation impacts the behavior of other immune and non-immune stromal cells found within the breast TME.

Here we show that host phospho-eIF4E has a pleiotropic effect in the TME of an animal model of PPBC, regulating the functions of fibroblasts and ILC2, two cell types important for the metastatic process. The altered functionality of fibroblasts, in turn, differentially affects tumor cells, to support the immune evasion and metastasis of PPBC tumors. We show that immune composition of both the primary tumor and metastatic niche is altered in the phospho-eIF4E-deficient animals. In a pioneering approach, using Imaging Mass Cytometry on a cohort of human PPBC and non-PPBC tumors, we show that the human PPBC TME is characterized by

markers of immune dysfunction. Finally, we provide evidence for a potential therapeutic intervention in PPBC, by showing that the combination of the MNK1/2 inhibitor SEL201 and PD-1 blockade decreases lung metastasis in a murine model of PPBC.

Methods

Mouse Model

Wild-type (WT) BALB/c and C57BL/6N mice were purchased from Charles River Laboratory. eIF4E$^{S209A/S209A}$ BALB/c and eIF4E$^{S209A/S209A}$ C57BL/6N mice were gifts from Dr. Nahum Sonenberg at McGill University and have been previously described (13). PPBC models were set up as previously reported (19). Briefly, 5- or 6-week old WT or eIF4E$^{S209A/S209A}$ female mice were mated with male mice. Pregnant mice were monitored until pups were born and allowed to lactate for 11 to 14 days. The pups were removed from the dams causing the dams to undergo forced weaning-induced mammary gland involution. On involution day 1, that is twenty-four hours post-forced weaning, 200,000 66cl4 cells were injected into the inguinal mammary gland of BALB/c mice and tumors were allowed to grow for 14 (early metastasis) or 33 days (full metastasis) (Fig. 1A). 200,000 E0771 cells were injected into the mammary gland of C57BL/6N mice for 26 days. For drug treatment experiments, animals were treated at time points indicated in the schematic illustration (Supplementary Fig. S6D), starting at 4 days post-tumor cell injection. SEL201 (Ryvu Therapeutics) was dissolved in DMSO and then diluted in N-Methylpyrrolidone (NMP, Fisher Scientific) and Captisol (Ligand) for administration by oral gavage at 75 mg/kg bodyweight per mouse per day, 5 days per week (with 2 days off) for 3 weeks (a total of 15 doses). The anti-mouse PD-1 monoclonal antibody and IgG isotype control (BioCell) were diluted in PBS and administrated through intraperitoneal injection at 10 mg/kg bodyweight per mouse per day, once per week for 3 weeks (a total of 3 doses). Animal experiments were conducted following protocols approved by McGill University Animal Care and Use Committee.

Cells and Reagents

SEL201 was a generous gift from Dr. Tomasz Rzymski at Ryvu Therapeutics. The 66cl4 and MDA-MB-231 cell lines were kind gifts from Dr. Josie Ursini-Siegel at McGill University. The E0771 cell line was purchased from CH3 BioSystems. All cell lines used are routinely (every 3 months) tested for mycoplasma using the eMyco plus mycoplasma PCR detection kit (LiliF Diagnostics). Cells were injected into animals no later than 4-5 passages after thawing. 66cl4 was cultured in RPMI with 10% FBS and antibiotics (1x pen/strep, wisent). E0771 was cultured in RPMI supplemented with 10mM HEPES, 10% FBS and antibiotics. WT and eIF4E$^{S209A/S209A}$ (referred to as eIF4E^{S209A}) primary mammary gland fibroblasts were obtained by digesting minced mammary glands pooled from 3-4 donor mice in 1 mg/ml Collagenase IV in DMEM Advanced F12 for 1h at 37 °C, passing the suspension through a 70 µm cell strainer and centrifuging at 300g for 10 minutes. The pelleted cell suspension including fibroblasts was plated in DMEM supplemented with 10% FBS and antibiotics. To enrich for fibroblasts, culture medium was changed 30 minutes after plating, by removing old media and non-adherent cells and adding fresh media. Cells were expanded for 8-9 days. Conditioned media was prepared by thoroughly washing away culture media and culturing the fibroblasts in serum-free DMEM F12 for 48h. Presence of secreted IL-33 in the conditioned media was visualized on a Proteome Profiler Mouse XL Cytokine Array (R&D Systems). The concentration of IL-33 secreted in the conditioned medium was measured on a V-PLEX Mouse Cytokine 19-Plex Kit (Meso Scale Diagnostics) and normalized to total protein input measured by Nanodrop. WT and eIF4E$^{S209A/S209A}$ (termed eIF4E^{S209A}) mouse embryonic fibroblasts (MEFs) have been described previously (13,15). Cancer-associated fibroblasts (CAFs) derived from patients with breast cancer were obtained in collaboration with Dr. Mark Basik at McGill University as previously described (20). The collection and use of human tissues was approved by the Institutional

Review Board (IRB), JGH (No. 05-006), which is in accordance with the Declaration of Helsinki and the Belmont Report. CAFs and MDA-MB-231 cells were cultured with DMEM supplemented with 10% FBS and antibiotics (1x pen/strep, wisent).

Circulating tumor cell quantification

Tumor-bearing PPBC mice were sacrificed by cardiac puncture at day 14 of tumor growth and equal volumes/animal of peripheral blood were collected into EDTA-coated tubes. After treatment with red blood cell lysis buffer (Sigma-Aldrich) to selectively deplete erythrocytes and centrifugation, the cell pellet was resuspended in RPMI containing 5 mg/L 6-thioguanine (Sigma-Aldrich), plated in one well/animal of a 6-well plate and cultured at standard tissue culture conditions (37 °C 5% CO_2). After one week, surviving 6-thioguanine resistant cells (circulating 66cl4 cells) were counted using a brightfield microscope under a 10x magnification. For each animal, cell numbers in 4 individual fields of view were counted and the sum shown as tumor cells per 500 ul collected blood.

Immunophenotyping

Lungs and tumors were resected from sacrificed animals at indicated time points and digested into a single cell suspension via mechanical mincing into small pieces and incubation with collagenase IV (1 mg/ml) in RPMI medium (Gibco) for 1h at 37 °C. After treatment with red blood cell lysis buffer to selectively deplete erythrocytes, cells were counted, blocked with anti-CD16/32 and stained with indicated antibodies (Supplementary Table S1). Flow cytometry data was acquired on a BD LSRFortessa flow cytometer (BD Biosciences) and analyzed with FlowJo software, version 10.7.1 (BD Biosciences). The gating strategies used for analysis are found in Supplementary Fig. S2.

ILC2 isolation

ILC2Ps, the progenitors of ILC2s, were isolated from bone marrow and expanded as previously reported (21). AlamarBlue Cell Viability assay was performed according to manufacturer's instructions (Thermo Fisher Scientific), and the absorbance was subsequently measured for cell division with excitation and emission wavelengths at 560nm and 590nm respectively as previously reported (21). IL-5 and IL-13 secretion by ILC2s was quantified by ELISA as previously reported (21). For annexin V and live dead staining, cells were seeded at 10,000 cells/well in complete media and cytokine-starved for 3 hours prior to cytokine stimulation and drug inhibition. This was followed by addition of 0.5 micromolar, 2.5 micromolar, or 5 micromolar SEL201, or DMSO with respective cytokines (10 ng/mL). After 5 days, cells were stained with Annexin V Apoptosis Detection Kit (eBioscience) according to the manufacturer's protocols and eFluor 780 Fixable Viability Dye (eBioscience). Data were acquired using a BD LSRFortessa™ flow cytometer.

Migration and Invasion and co-culture assays

66cl4 and E0771 cells were seeded at one (migration and invasion assay) or two (co-culture assay) million cells per 10 cm dish on day 1 in full media, then starved overnight by switching to serum-free media on day 2. For the co-culture assay, 200,000 WT or eIF4E^{S209A} mouse embryonic fibroblasts were seeded into 12-well companion plates on day 2. On day 3, transwells (Corning) were coated with Collagen I (20 μg/ml) as previously reported (22). 200,000 (migration and invasion) or 50,000 (co-culture assay) tumor cells were seeded into the transwells and were allowed to migrate and invade for 16h (migration and invasion) or 48h (co-culture). Migrated cells were fixed with 5% glutaraldehyde (Sigma) and stained with 0.5% crystal violet (Sigma) as previously reported (22). Stained cells were then counted and quantified. WT and eIF4E^{S209A} fibroblasts were harvested for WB or qPCR

For experiments with patient-derived CAFs, MDA-MB-231 cells were seeded at 3 million cells per 10cm dish on day 1 in full media, then switched to serum-free media on day 2 and starved overnight. 50,000 patient-derived CAFs were seeded into 6-well companion plates on day 2. On day 3, transwells were coated with Collagen I (20 μg/ml). 200,000 MDA-MB-231 cells were seeded into the transwells and were allowed to migrate and invade towards CAFs for 48h. Migrated cells were fixed, stained and quantified as described above. CAFs were harvested for WB.

Immunohistochemistry (IHC) and H&E staining

Immunohistochemistry and hematoxylin and eosin (H&E) staining were performed as previously described (22). Briefly, tumor and lung sections were stained for IL-33, phospho-eIF4E and CD8, and counterstained with 20% Harris-modified hematoxylin (Fisher). Antibody information is listed in Supplementary Table S2. Slides were scanned and assessed using Spectrum (Aperio Technologies). All animal and patient IHC samples were quantified by QuPath software.

Immunofluorescence (IF)

IF staining was performed as previously described (23). Briefly, cells or tissues were stained for the indicated proteins, and nucleus were labeled with DAPI. Primary and secondary antibodies are listed in Supplementary Table S2. Slides were scanned with an axioscan Z1 slide scanner microscope (Zeiss) using a 20x/0.75NA objective. Images were analyzed using Zen blue software (Zeiss) and Qupath.

Western Blotting

Cells were lysed with RIPA buffer (150 mmol/L Tris-HCl, pH 7, 150 mmol/L NaCl, 1% NP-40, 1% sodium deoxycholate, 0.1% SDS) supplemented with protease and phosphatase inhibitors (Roche) as previously described (22,24). Equal amounts of protein were loaded and separated on

10% SDS-PAGE gels. Antibodies were used to detect the indicated proteins. GAPDH was probed to confirm equal protein loading. Antibody information is listed in Supplementary Table S2. **Quantitative PCR**

RNA was prepared using E.Z.N.A. total RNA isolation kit (OMEGA Bio-Tek). cDNA was prepared from 1 μg of total RNA, using iScript cDNA Synthesis Kit (Bio-Rad). Target genes were quantified using the Applied Biosystems 7500 Fast Real-Time PCR System with SYBR Green. Primers are listed in Supplementary Table S3.

RNA interference

ST2 knockdown in 66cl4 cells was performed as previously described (25). Briefly, scramble siRNA (AllStars Negative Control siRNA, Qiagen) or ST2 siRNA (IDT, sequences listed in Supplementary Table S4) were introduced into 66cl4 cells with the aid of lipofectamine RNA iMax reagents (Invitrogen) following the manufacturer's instructions.

Whole-mount analysis of mammary glands

Mammary glands from BALB/c eiF4E^{WT} and BALB/c eIF4E^{S209A} at day 8 after pregnancy (LD8) and day 2,3,4,5 and 6 after weaning (ID2, ID3, ID4, ID5, ID6 respectively) were collected, fixed in Carnoy's fixative, defatted one time with xylene and stained in carmine red solution overnight. Tissues were dehydrated in increasing concentrations of ethanol, (70%, 95% and 100% respectively), then cleared in xylene and mounted with Permount. Pictures were taken on a surgical microscope at 25X. The average percentage of the area occupied by adipocytes compared to epithelial cells of 5 random fields at the indicated time points was quantified using ImageJ.

Data acquisition by IMC

The study was approved by the ethics committee and in compliance with institutional review board approval from the 2 participating institutions: UZ/KU Leuven (Belgium) and Jewish General Hospital (Canada). Written informed consent was obtained from all patients (nulliparous breast cancer samples, breast cancer samples from patients diagnosed during pregnancy or diagnosed postpartum) and the study conducted in accordance with the Declaration of Helsinki. Human breast cancer samples were arrayed onto a slide, stained using the panel of antibodies listed in Supplementary Table S5, and processed with the Hyperion Imaging System (Fluidigm) by the Single Cell Imaging and Mass Cytometry Analysis Platform (SCIMAP) of the Goodman Cancer Research Centre, McGill University, according to their guidelines. Areas of dimension 1000 x 1000 µm were acquired for 23 sample cores. The resulting data files were stored in MCD binary format.

Statistical Analysis

Software (GraphPad) was used to determine statistical significance of differences. Normality of data was evaluated by using the Shapiro-Wilk test. Normal data were interpreted using unpaired Student's t-test, one-way ANOVA followed by the Tukey post hoc test for multiple comparisons or two-way ANOVA followed by the Tukey post hoc test for multiple comparisons. Non-normal data were interpreted using Mann-Whitney test. P values < 0.05 were considered significant. The details of statistical analysis for each experiment are listed in Supplementary Tables S6-S7.

Results

Loss of eIF4E phosphorylation in the stroma protects against PPBC lung metastasis

We have previously reported that the absence of phospho-eIF4E in both tumor and stromal cells is sufficient to reduce lung metastasis in the PyMT transgenic model of breast cancer (15). To dissect the importance of stromal phospho-eIF4E specifically in PPBC, we investigated whether stromal phospho-eIF4E deficiency is sufficient to block metastasis in a pre-clinical mouse model of this disease. Using the involuting mammary gland as an experimental platform to model PPBC metastasis, 66cl4 murine breast cancer cells were injected into the inguinal mammary glands of wild-type (WT) or $eIF4E^{S209A/S209A}$ (phospho-eIF4E null, henceforth termed $eIF4E^{S209A}$) BALB/c mice one day following weaning-induced involution (Fig. 1A). Consistent with previously published data, tumor cells injected into the involuting mammary gland are more metastatic, compared to the same tumor cells injected into virgin mammary glands of age-matched mice (Supplementary Fig. S1A). In the PPBC model, we did not observe a difference in primary tumor outgrowth between WT and $eIF4E^{S209A}$ PPBC mice, as both tumor initiation, growth and weight at endpoint were similar (Fig. 1B, Supplementary Fig. S1B and S1C). Strikingly, we observed a significant decrease in lung metastases in $eIF4E^{S209A}$ PPBC mice, that is, mice devoid of phosphorylated eIF4E, compared to their WT PPBC counterparts (Fig. 1C). Moreover, there were fewer tumor cells detected in the circulation of $eIF4E^{S209A}$ PPBC mice on day 14 of tumor growth (Fig. 1D), suggesting a defect in tumor extravasation. Ki67 staining of lung metastases showed no difference in the percentage of Ki67 positive cells in the WT and $eIF4E^{S209A}$ lungs (Fig. 1E), indicating similar tumor cell proliferation at the pulmonary metastatic site. Similar results were obtained when E0771 murine breast cancer cells, syngeneic

to C57BL/6 mice, were injected into the involuting mammary glands of WT or eIF4E^{S209A} (Fig. 1F and G, Supplementary Fig. S1D-S1G).

Myeloid cells expressing CD11b (marker for myeloid cells) and Gr1 (granulocyte marker present in both Ly6G and Ly6C molecules) are known to increase at pre-metastatic niches and support metastasis (16,26). Given the differences in the metastatic burden in the lung, but not primary tumor outgrowth, observed between WT and eIF4E^{S209A} PPBC mice, we focused on whether phospho-eIF4E deficiency at the lung metastatic site altered the infiltration of CD11b^{+}, Ly6G^{+}, Ly6C^{+} myeloid cell populations. We employed multi-color flow cytometry to immune phenotype the tumor-bearing lungs and discovered a significant reduction in granulocytes (CD45^{+}CD11b^{+}Ly6G^{+}Ly6C^{lo}) and elevation of CD8^{+} T cells in the lungs of eIF4E^{S209A} PPBC mice at the experimental endpoint of the tumor model, 33 days post tumor injection. (Fig. 1H, and Supplementary Fig. S2 for gating strategies). However, the pulmonary levels of monocytic cells (CD45^{+}CD11b^{+}Ly6G^{-}Ly6C^{hi}) were similar between WT and eIF4E^{S209A} PPBC mice (Fig. 1H). These differences in immune cell infiltrates arise as a consequence of tumor development, as similar changes were not detected in the lungs of age-matched naïve animals (Supplementary Fig. S1H). In conclusion, during tumor progression, phospho-eIF4E deficiency in the host reduces pulmonary recruitment of myeloid cells that support metastasis, increases the presence of CD8^{+} T cells, and impairs lung metastasis.

Mammary gland involution is characterized by the elimination of milk-secreting mammary epithelia and the re-population of adipocytes. We next addressed whether the reduced metastatic burden in the lungs of eIF4E^{S209A} PPBC mice was due to a defect in their ability to undergo the physiologic process of mammary gland involution. We quantified the ratio of adipocytes over epithelial cells at lactation day 8, involution days 2, 4, and 6 in WT and

eIF4E^{S209A} mice. The adipocyte/epithelium ratio increases in a similar pattern over the course of WT and eIF4E^{S209A} mammary gland involution (Supplementary Fig. S1I), and WT and eIF4E^{S209A} show similar gross morphology during involution (Supplementary Fig. S1J). Phosphorylation of STAT3 is known to be induced and required for mammary gland involution (27), thus we also examined the levels of phospho-STAT3 in the WT and eIF4E^{S209A} mice, but found no difference in STAT3 phosphorylation (Supplementary Fig. S1K). Together, these results suggest that mice devoid of phospho-eIF4E undergo the physiological process of involution similarly to their WT counterparts. Thus, the reduced metastasis observed in phospho-eIF4E null PPBC mice is not the result of overt defects in mammary gland involution.

Phosphorylated eIF4E regulates IL-33 expression in fibroblasts to support breast cancer cell invasion

Tumor cell invasion and metastasis are regulated to a large degree by molecular signals that can originate within the primary tumor microenvironment (TME). We hypothesized that the reduction in metastatic colonies observed in the lungs of the eIF4E^{S209A} PPBC mice is reflective of a differential expression of such signals in the TME of phospho-eIF4E-deficient hosts. Recently, the IL-33/ST2 signaling axis has been implicated as a potent modulator of the TME, regulating the recruitment and activation of immune cells as well as tumor cell invasiveness (28-31). We performed IHC on the 66cl4-derived primary tumors that were grown for 2 weeks either in WT or eIF4E^{S209A} PPBC mice, and found that IL-33 levels are lower in the tumors grown in eIF4E^{S209A} PPBC mice, compared to those tumors derived from WT PPBC mice (Fig. 2A). Moreover, the expression of phospho-eIF4E correlates with IL-33 expression in WT PPBC tumors (Fig. 2B).

Next, we sought to determine the cellular components in the PPBC tumors that produce IL-33. Fibroblasts become activated during mammary gland involution, and they support PPBC invasion and metastasis, in part, via their active secretome (32). We thus sought to determine whether fibroblasts were a major source of IL-33 in our PPBC model. We isolated primary fibroblasts from the mammary glands of WT and eIF4E^{S209A} mice, expanded them *ex vivo* and analyzed their secretome. Mammary fibroblasts derived from eIF4E^{S209A} mice were found to secrete lower levels of IL-33 compared to WT cells (Fig. 2C and D). We also exploited mouse embryonic fibroblasts (MEFs) derived from WT or eIF4E^{S209A} mice as an additional tool to confirm that the phosphorylation of eIF4E was indeed required for the regulation of IL-33 protein expression (Fig. 2E).

IL-33 has been shown to directly impact invasion and metastasis via binding its receptor ST2, which is encoded by interleukin 1 receptor-like 1 (*Il1rl1*) on tumor cells (29,33). Hence, we sought to determine whether fibroblast-derived IL-33 positively supports breast tumor cell invasion. We used a co-culture model system to study interactions between fibroblasts and the 66cl4 and E0771 breast cancer cells used in our *in vivo* PPBC models (Fig. 2F). When 66cl4 or E0771 breast cancer cells were co-cultured with WT or eIF4E^{S209A} fibroblasts, both breast cancer cell lines displayed a decreased propensity to invade through a Collagen I matrix in the presence of the eIF4E^{S209A} fibroblasts, as compared to WT fibroblasts (Fig. 2G, Supplementary Fig. S3A). We also observed a robust increase in the expression of fibroblast-derived IL-33 mRNA and protein when we cultured breast cancer cells in the presence of fibroblasts, however eIF4E^{S209A} fibroblasts still express significantly less IL-33 mRNA and protein, as compared to their WT counterparts (Fig. 2H and I, Supplementary Fig. S3B and S3C).

As we observed that breast cancer cells display an increased propensity to invade toward WT fibroblasts compared to eIF4E^{S209A} fibroblasts, we next examined whether we could pharmacologically inhibit this process using the MNK1/2 inhibitor SEL201 (34). WT fibroblasts were treated with SEL201, and co-cultured with either 66cl4 or E0771 cells. Concomitant with repressed phospho-eIF4E expression in fibroblasts, SEL201 treatment decreased IL-33 protein levels in WT fibroblasts (Fig. 2J, Supplementary S3D). Moreover, the invasion of 66cl4 and E0771 cells was less robust when co-cultured with SEL201-treated fibroblasts (Fig. 2K, Supplementary Fig. S3E).

Finally, we addressed the clinical relevance of our findings by co-culturing patient-derived CAFs with MDA-MB-231 human breast cancer cells. We obtained primary CAFs that were isolated from the freshly resected human breast tumors of four patients. Primary CAFs were treated with vehicle or SEL201, and subsequently co-cultured with MDA-MB-231. Similar to our findings in the murine fibroblasts, SEL201 repressed phospho-eIF4E and IL-33 expression in patient-derived CAFs, and MDA-MB-231 invaded less robustly in the presence of SEL201-treated CAFs (Fig. 2L and M). Collectively, our data show that IL-33 expression in fibroblasts is regulated by the MNK1/2-eIF4E axis.

IL-33 activates the MNK1/2-eIF4E pathway downstream of activated ST2 to support an immune suppressed TME

Having shown the important role of fibroblast-derived IL-33 in supporting breast cancer cell invasion, as well as the reduction of IL-33 in the TME of eIF4E^{S209A} PPBC tumors, we next investigated whether fibroblast-derived IL-33 acts via the IL-33 receptor, ST2, expressed on 66cl4 cells, to promote breast cancer invasion. By ablating the expression of *Il1rl1* using siRNA in 66cl4 cells, we observed an impaired ability of the ST2-deficient tumor cells to invade in the

presence of WT fibroblasts (Fig. 3A, Supplementary Fig. S4A). Such data indicate that fibroblast-derived IL-33 signals in a paracrine fashion to ST2-expressing breast cancer cells to augment tumor cell invasion. Therefore, we chose to further dissect how IL-33 signals downstream of ST2 in breast tumor cells, focusing on the p38 and ERK1/2 MAPK signaling proteins, which lie immediately upstream of MNK1/2 activation (14). Stimulation of 66cl4 cells with recombinant murine IL-33 (rIL-33) resulted in increased phosphorylation of both p38 MAPK and eIF4E, but not phosphorylation of ERK1/2 (Fig. 3B, Supplementary Fig. S4B), and promoted 66cl4 (Fig. 3C) and E0771 invasion (Supplementary Fig. S4C). Additionally, we hypothesized that IL-33 might stimulate the expression of pro-inflammatory and pro-tumorigenic cytokines/chemokines in tumor cells, which may further remodel the TME to favor invasion. rIL-33 stimulated the mRNA expression of *Cxcl1, Ccl17, Csf2* (which encodes GM-CSF) and *Il6*, without significantly affecting *Il4* and *Cxcl2* levels (Fig. 3D). Finally, a main immune cell type whose expansion is reliant on IL-33/ST2 signaling, and which have been shown to play an important role in tumor immunity, are ILC2 cells (8). Using *ex vivo* expanded ILC2s from the bone marrow of BALB/c mice, we examined their cellular proliferation as well as their ability to secrete IL-5 and IL-13 in response to the co-stimulation with rIL-7 plus rIL-33 in the presence and absence of SEL201 (21). SEL201 treatment of ILC2s reduced their secretion of IL-5 and IL-13, in response to combined rIL-7 and rIL-33 (Fig. 3E). Although we observed minimal effects of SEL201 on the proliferation of ILC2 cells (Fig. 3F), their viability was significantly inhibited (Supplementary Fig. S4D). Together, these results suggest that blocking the phosphorylation of eIF4E in ILC2 cells ultimately negatively impacts their secretion of IL-5 and IL-13, which are important for the recruitment of $CD11b^{+}Gr1^{+}$ cells (7-10,35-38). In toto, given the reported functions of CXCL-1, CCL-17, GM-CSF, IL-6, IL-5 and IL-13 in tumor immune evasion

(36,37,39-47), our data provide evidence that IL-33 may serve to create an immunosuppressive PPBC TME to facilitate metastasis in a MNK1/2-phospho-eIF4E-dependent way.

Characterization of the human and murine PPBC TME

The expression of phospho-eIF4E positively correlates with IL-33 protein level in 66cl4 tumors grown in WT PPBC mice (Fig. 2B). To interrogate whether these observations are clinically relevant, we used immunofluorescence (IF) staining to evaluate the expression of phospho-eIF4E and IL-33 in a cohort of PPBC patient samples. Consistent with our PPBC murine data, phospho-eIF4E expression correlates with IL-33 levels in human PPBC tumors (Fig. 4A). To verify the broader implications of our observations, we examined TCGA data using UCSC Xena (http://xenabrowser.net/) for the relationship between MNK1 and IL-33 expression. We found that *MKNK1* and *IL33* mRNA levels significantly correlate with one another (Fig. 4B).

The limited success of immune targeted therapy in breast cancer, relative to other malignancies, has been attributed in part to the heterogeneity of the breast TME. The TME of human PPBC has not been well defined, and we used CyTOF imaging mass cytometry (IMC) to simultaneously quantify the expression of 26 proteins within the TME of nulliparous breast cancer (BC), breast cancer diagnosed during pregnancy (PrBC), and postpartum breast cancer (PPBC) (Supplementary Table S8 and Supplementary Fig. S5A). We report that PrBC and PPBC differ from BC primarily in the relative proportion of tumor cells and immune cells, as well as their level of activation of the MNK1/2-eIF4E axis. Phospho-eIF4E, eIF4E, and MNK1 were detectable in tumor cells, immune cells, fibroblasts, pericytes, and endothelial cells (Fig. 4C and Supplementary Fig. S5B-S5D). In particular, the tumor cell population in PPBC and PrBC showed a significantly increased level of phospho-eIF4E expression, compared to the tumor cells

represented in BC (Fig. 4D). Furthermore, PD-L1 was expressed in tumor cells regardless of the cancer subtype, with PD-L1 expression being significantly increased in PPBC tumor cells compared to PrBC tumor cells (Fig. 4D). Moreover, when we examined tumor cells with the highest expression of phospho-eIF4E (99^{th} percentile), the expression of PD-L1 was most abundant in PPBC, compared to BC and PrBC (Supplementary Fig. S5E). CD8 is an important tumor immune biomarker, so we next investigated the proportion of $CD8^+$ T cells in the three patient cohorts. We observed a significant increase in $CD8^+$ T cells in the PPBC samples, and the phosphorylation of eIF4E is significantly increased in the $CD8^+$ T cells present in PPBC, compared to BC or PrBC samples (Fig. 4E). Further characterization of the phenotype of the $CD8^+$ T cells showed that the co-expression of HLA-DR and PD-1 was significantly higher in PPBC samples, compared to $CD8^+$ T cells present in PrBC or BC (Fig. 4F). As HLA-DR is known to be expressed on activated T cells, and PD-1 is an exhaustion marker, our data suggest that the $CD8^+$ T cells present in PPBC express an activated dysfunctional phenotype (48,49), although we note that we cannot test the functionality of HLA-$DR^+$$PD\text{-}1^+$ T cells identified in the archived PPBC samples by IMC. These human data did, however, prompt us to profile the TME in the PPBC murine model early in tumorigenesis (i.e. day 14 post tumor cell injection). We observed that the recruitment of various immune cell subsets in the TME of the PPBC mice was not affected by phospho-eIF4E deficiency (Supplementary Fig. S5F-S5H). However, immune phenotyping using multi-color flow cytometry revealed that phospho-eIF4E competent WT PPBC mice contained fewer IFNγ- and CD107a-expressing tumor-infiltrating T cells (both activation markers), compared to phospho-eIF4E-deficient mice (Fig. 4G). In addition, the expression level of the T cell co-stimulatory molecule CD86 was found to be lower on dendritic cells in WT PPBC mice compared to phospho-eIF4E null PPBC mice (Supplementary Fig. S5I).

Thus, immune characterization of the TME in both human and murine PPBC tumors suggests an association between phospho-eIF4E activity in the TME and T cell phenotypes.

Dual MNK1/2 and PD-1 blockade inhibits PPBC lung metastasis

The efficacy of immune checkpoint inhibitors in metastatic breast cancer, including PPBC, would likely be improved by overcoming tumor immune escape. We observed that the lungs of tumor-bearing phospho-eIF4E-deficient animals were infiltrated by higher numbers of cytotoxic $CD8^+$ cells at day 14 of tumor growth, prior to overt metastasis (Fig. 5A, Supplementary Fig. S6A). Proportions of $CD11b^+Ly6C^+$ and $CD11b^+Ly6G^+$, as well as total $CD3^+$ cells were unchanged at this time point (Supplementary Fig. S6B). Within the $CD8^+$ population, in turn, more cells were positive for the IFNγ, a marker of T cell activation, at day 14 of tumor growth (Fig. 5B), an effect that is not observed in the lungs of non-tumor bearing animals (Supplementary Fig. S6C). These data suggest that phospho-eIF4E can contribute to PPBC immune evasion during the establishment of the metastatic niche. We thus hypothesized that SEL201 might sensitize PPBC mice to the anti-metastatic effects of PD-1 blockade. To test this hypothesis, WT PPBC mice were administered vehicle, SEL201, anti-PD-1 antibody, or the combination of SEL201 plus anti-PD-1 antibody (Supplementary Fig. S6D). These drug treatments did not significantly affect tumor growth (Fig. 5C, Supplementary Fig. S6E). Intriguingly, SEL201 plus anti-PD-1 blockade decreased PPBC lung metastasis, while SEL201 or anti-PD-1 alone did not show any significant anti-metastatic effects (Fig. 5D). However, SEL201 treatment alone resulted in a significant decrease in phospho-eIF4E expression, suggesting efficient target engagement by the MNK1/2 inhibitor, and a robust increase in $CD8^+$ cells in the lung metastases (Supplementary Fig. S6F, Fig. 5E), which was not enhanced by

addition of anti-PD-1. Administration of SEL201 or anti-PD-1 did not have any overt systemic toxicity (Supplementary Fig. S6G), consistent with our previous work (22,50). Thus, targeting the MNK1/2-eIF4E axis might have therapeutic benefit for augmenting the efficacy of immunotherapy in women diagnosed with PPBC.

Discussion

Metastasis associated with PPBC and mortality due to lack of effective treatment strategies necessitate a fuller understanding of this disease (51,52). Recent breakthroughs in immune checkpoint blockade therapies have stimulated research to better understand the TME of breast cancer, aiming to discover possible approaches to sensitize metastatic breast cancer to immunotherapies. Here, we demonstrated the central role of stromal phospho-eIF4E in promoting pro-tumorigenic immunity in a model of metastatic PPBC (graphical abstract). Collectively, our work highlights the important role of the IL-33-MNK1/2-eIF4E axis in PPBC invasion and metastasis by impacting multiple cellular compartments in the TME. IL-33 might hold potential as a therapeutically targetable cytokine in PPBC, and perhaps more broadly in breast cancer.

The regulation of IL-33 by the MNK1/2-eIF4E axis is potentially relevant for immune cell function, as IL-33 is known to reinforce pro-tumorigenic inflammation (53). Within the immune cell compartment, IL-33 has important effects on numerous cell types such as eosinophils, mast cells and ILC2s (4,31,54). IL-33 is essential for the polarization of ILC2s together with IL-7, IL-25 and TSLP (55). Our understanding of the roles ILC2 plays in the context of tumor biology is still rudimentary, although recent studies have described their tumor-promoting and anti-tumor roles in several cancer types, including breast cancer (9,10,56,57). In our study, we showed that the pharmacologic inhibition of MNK1/2 blocked the IL-33-induced

expression of *ex vivo* expanded ILC2-derived cytokines IL-5 and IL-13. We have yet to test whether hosts devoid of phospho-eIF4E, which presented with less granulocytic $CD45^{+}CD11b^{+}Ly6G^{+}Ly6C^{lo}$ cells in the lungs, is due to suppression of the IL-33-ILC2-MDSC axis (10). In addition, our study has expanded the repertoire of IL-33-induced pro-inflammatory cytokines and chemokines (i.e., *Cxcl1*, *Ccl17*, *Il6* and *Csf2*) produced by tumor cells. The significance of these four factors in tumor immune evasion has been supported by multiple previous reports. For example, over-expression of CXCL-1 and its receptor CXCR-2, as well as elevated circulating IL-6 levels, are all correlated to breast cancer metastasis and poor survival rate (58,59), and CXCL-1, IL-6 and GM-CSF are all potent mediators for the recruitment and expansion of MDSCs and M2-like macrophages (41-43,45). CCL-17, an important ligand for CCR-4, has also been demonstrated to elicit Th2 and T_{reg}-mediated cancer immune evasion (39,44). Taken together, we show that IL-33 acts directly on ILC2 and breast tumor cells to induce the expression of selected immunosuppressive chemokines and cytokines.

In addition to its impact on immune cells, IL-33 has also been reported as a pro-tumorigenic and pro-invasive cytokine (28-30). Elevation of IL-33 was observed in the serum of breast cancer patients (60,61). Moreover, the levels of matrix metallopeptidase 11 (*MMP11*), a pro-invasive enzyme responsible for tissue remodeling, are directly correlated with *IL33* levels in patients with breast cancer (61), supporting a possible pro-invasive function of IL-33. In this context, we have demonstrated that tumor-bearing phospho-eIF4E-deficient mice have fewer tumor cells in circulation. Disrupting IL-33/ST2 signaling *in vitro* diminished the ability of cancer cells to invade. Thus, our data highlight the crosstalk between cancer cells and fibroblasts, whereby cancer cells educate fibroblasts to secrete more IL-33, thus allowing breast

cancer cells to gain more invasive properties and implicate the MNK1/2-phospho-eIF4E axis as the driver of this crosstalk.

Interestingly, in the preparation of this manuscript, a study was published linking IL-33 derived from fibroblasts at the metastatic site to type 2 immunity, leading to a fecund microenvironment for cancer cell colonization (31). Their study showed that targeting IL-33 can reduce metastasis in the 4T1 murine model of breast cancer, which is consistent with the results presented herein. It should be noted that in our study, we report a potentially important role of fibroblast-produced IL-33 at the primary tumor site to facilitate tumor cell extravasation. Moreover, IL-33 may give rise to systemic changes in cytokine production, directly or indirectly causing down-stream effects on immune cell recruitment to the lungs. As we see increased expression of type I immunity activation markers in the T cells at both the primary site and lung in the phospho-eIF4E-deficient animals, our overall conclusions regarding pro-tumor IL-33 strengthen the potential of MNK1/2 inhibitors, IL-33 targeting agents, and immunotherapy in clinical applications.

Immune checkpoint blockades designed to release the brakes on exhausted cytotoxic T cells have largely improved the patient prognosis in several cancers (62), but are less effective to date in breast cancer. It is proposed that many breast cancers display failed or suboptimal T cell priming. Specifically in PPBC, increase in PD-1 expression on T cells and efficacy of anti-PD-1 treatment in reversing involution-associated tumor growth was recently reported (63). In line with this finding, we observe increased expression of PD-1 on the tumor-infiltrating $CD8^+$ cells in PPBC patients. We propose, although we have not evaluated this claim experimentally, that in the TME of PPBC tumors, these cells present a dysfunctional immunosuppressive phenotype. In this context, it is interesting that these $CD8^+$ cells also express elevated levels of phospho-eIF4E.

While the role of phospho-eIF4E in regulating functionality of specifically $CD8^+$ has not yet been explored by the scientific community and is beyond the scope of this present study, emerging data suggest that the activity of MNK1/2-eIF4E axis in immune cells affects their function. For example, a recent paper reported that the immunosuppressive phenotype of bone-marrow derived macrophages is governed by the MNK1/2-eIF4E axis and can be reversed by MNK2 inhibition, indirectly leading to increased $CD8^+$ cell activation (17). Furthermore, a pre-clinical study of the MNK1/2 inhibitor Tomivosertib (eFT508) in liver cancer has shown that this inhibitor enhances the activity of checkpoint inhibitors in a T-cell dependent manner, leading to an anti-tumor immune response (64). In summary, we propose that MNK1/2 inhibitors may convert “cold” breast tumors to “hot” tumors, thus offering the opportunity for immune checkpoint blockade to become more effective in highly metastatic cancers such as PPBC. This study, as well as others showing effects of MNK1/2 inhibition on cells of the TME (16,18), provide strong preclinical support to ongoing clinical testing of MNK1/2 inhibitors in breast cancer. Indeed, we are participating in a Stand Up to Cancer trial to test this question (ClinicalTrials.gov NCT04261218).

Acknowledgements:

We thank Christian Young (LDI Flow Cytometry facility), Kathy Forner and Veronique Michaud (LDI Imaging and Phenotyping Core), Dr. Naciba Benlimame, and Lilian Canetti for experimental advice and technical support. We thank Dr. Pepper Schedin (Oregon Health & Science University) and Dr. Qiuchen Guo (Harvard Medical School) for helpful discussion and experimental design.

This research is funded by the Canadian Institutes for Health Research (grants MOP-142281 to WHM, and PJT-156269 to WHM, SVDR and JHF, and grant PJT-162260 to SVDR and JHF) and the Cancer Research Society and CURE Foundation (grant 20239 to WHM). This work was also supported by a grant from McGill Interdisciplinary Initiative in Infection and Immunity (Mi4) to SVDR. The research was further supported by the Rossy Cancer Network. FA is senior researcher for the Research Fund Flanders (F.W.O.). Development of MNK1/2 inhibitor SEL201 was performed by Ryvu Therapeutics. QG was financed by a Cole Foundation Ph.D. fellowship, McGill Integrated Cancer Research Training Program (MICRTP) graduate studentship and a Ruth & Alexander Dworkin Ph.D. fellowship. MB is supported by the international postdoc grant from the Swedish Research Council (VR). FH was sponsored by MICRTP graduate studentships. SSK and SP are supported by FRQS doctorate fellowships. VZL was supported by MICRTP undergraduate studentship. HL was supported by a grant from the Flemish Cancer Society [3M150537]. WY was endowed the MICRTP graduate studentship.

References

1. Goddard ET, Bassale S, Schedin T, Jindal S, Johnston J, Cabral E, *et al.* Association Between Postpartum Breast Cancer Diagnosis and Metastasis and the Clinical Features Underlying Risk. *JAMA Netw Open* 2019;**2**(1):e186997 doi 10.1001/jamanetworkopen.2018.6997.
2. Schedin P. Pregnancy-associated breast cancer and metastasis. *Nat Rev Cancer* 2006;**6**(4):281-91 doi 10.1038/nrc1839.
3. Martinson HA, Jindal S, Durand-Rougely C, Borges VF, Schedin P. Wound healing-like immune program facilitates postpartum mammary gland involution and tumor progression. *Int J Cancer* 2015;**136**(8):1803-13 doi 10.1002/ijc.29181.
4. Liew FY, Girard JP, Turnquist HR. Interleukin-33 in health and disease. *Nat Rev Immunol* 2016;**16**(11):676-89 doi 10.1038/nri.2016.95.
5. Andersson P, Yang Y, Hosaka K, Zhang Y, Fischer C, Braun H, *et al.* Molecular mechanisms of IL-33-mediated stromal interactions in cancer metastasis. *JCI Insight* 2018;**3**(20) doi 10.1172/jci.insight.122375.
6. Chen SF, Nieh S, Jao SW, Wu MZ, Liu CL, Chang YC, *et al.* The paracrine effect of cancer-associated fibroblast-induced interleukin-33 regulates the invasiveness of head and neck squamous cell carcinoma. *J Pathol* 2013;**231**(2):180-9 doi 10.1002/path.4226.
7. Xiao P, Wan X, Cui B, Liu Y, Qiu C, Rong J, *et al.* Interleukin 33 in tumor microenvironment is crucial for the accumulation and function of myeloid-derived suppressor cells. *Oncoimmunology* 2016;**5**(1):e1063772 doi 10.1080/2162402X.2015.1063772.
8. Jovanovic IP, Pejnovic NN, Radosavljevic GD, Pantic JM, Milovanovic MZ, Arsenijevic NN, *et al.* Interleukin-33/ST2 axis promotes breast cancer growth and metastases by facilitating intratumoral accumulation of immunosuppressive and innate lymphoid cells. *International Journal of Cancer* 2014;**134**(7):1669-82 doi 10.1002/ijc.28481.
9. Chevalier MF, Trabanelli S, Racle J, Salome B, Cesson V, Gharbi D, *et al.* ILC2-modulated T cell-to-MDSC balance is associated with bladder cancer recurrence. *J Clin Invest* 2017;**127**(8):2916-29 doi 10.1172/JCI89717.
10. Trabanelli S, Chevalier MF, Martinez-Usatorre A, Gomez-Cadena A, Salome B, Lecciso M, *et al.* Tumour-derived PGD2 and NKp30-B7H6 engagement drives an immunosuppressive ILC2-MDSC axis. *Nat Commun* 2017;**8**(1):593 doi 10.1038/s41467-017-00678-2.
11. Ruggero D. Translational control in cancer etiology. *Cold Spring Harb Perspect Biol* 2013;**5**(2) doi 10.1101/cshperspect.a012336.
12. Robichaud N, Sonenberg N, Ruggero D, Schneider RJ. Translational Control in Cancer. *Cold Spring Harb Perspect Biol* 2019;**11**(7) doi 10.1101/cshperspect.a032896.
13. Furic L, Rong L, Larsson O, Koumakpayi IH, Yoshida K, Brueschke A, *et al.* eIF4E phosphorylation promotes tumorigenesis and is associated with prostate cancer progression. *Proc Natl Acad Sci U S A* 2010;**107**(32):14134-9 doi 10.1073/pnas.1005320107.
14. Prabhu SA, Moussa O, Miller WH, Jr., Del Rincon SV. The MNK1/2-eIF4E Axis as a Potential Therapeutic Target in Melanoma. *Int J Mol Sci* 2020;**21**(11) doi 10.3390/ijms21114055.

15. Robichaud N, Del Rincon SV, Huor B, Alain T, Petruccelli LA, Hearnden J, *et al.* Phosphorylation of eIF4E promotes EMT and metastasis via translational control of SNAIL and MMP-3. 2014 doi 10.1038/onc.2014.146.
16. Robichaud N, Hsu BE, Istomine R, Alvarez F, Blagih J, Ma EH, *et al.* Translational control in the tumor microenvironment promotes lung metastasis: Phosphorylation of eIF4E in neutrophils. *Proc Natl Acad Sci U S A* 2018;**115**(10):E2202-E9 doi 10.1073/pnas.1717439115.
17. Bartish M, Tong D, Pan Y, Wallerius M, Liu H, Ristau J, *et al.* MNK2 governs the macrophage antiinflammatory phenotype. *Proc Natl Acad Sci U S A* 2020;**117**(44):27556-65 doi 10.1073/pnas.1920377117.
18. Huang F, Goncalves C, Bartish M, Rémy-Sarrazin J, Issa ME, Cordeiro B, *et al.* Inhibiting the MNK1/2-eIF4E axis impairs melanoma phenotype switching and potentiates anti-tumor immune responses. *The Journal of Clinical Investigation* 2021 doi 10.1172/JCI140752.
19. Lyons TR, Borges VF, Betts CB, Guo Q, Kapoor P, Martinson HA, *et al.* Cyclooxygenase-2-dependent lymphangiogenesis promotes nodal metastasis of postpartum breast cancer. *J Clin Invest* 2014;**124**(9):3901-12 doi 10.1172/JCI73777.
20. Hosein AN, Wu M, Arcand SL, Lavallee S, Hebert J, Tonin PN, *et al.* Breast carcinoma-associated fibroblasts rarely contain p53 mutations or chromosomal aberrations. *Cancer Res* 2010;**70**(14):5770-7 doi 10.1158/0008-5472.CAN-10-0673.
21. Duerr CU, McCarthy CD, Mindt BC, Rubio M, Meli AP, Pothlichet J, *et al.* Type I interferon restricts type 2 immunopathology through the regulation of group 2 innate lymphoid cells. *Nat Immunol* 2016;**17**(1):65-75 doi 10.1038/ni.3308.
22. Guo Q, Li VZ, Nichol JN, Huang F, Yang W, Preston SEJ, *et al.* MNK1/NODAL signaling promotes invasive progression of breast ductal carcinoma in situ. *Cancer Res* 2019 doi 10.1158/0008-5472.CAN-18-1602.
23. Dahabieh MS, Ha Z, Di Pietro E, Nichol JN, Bolt AM, Goncalves C, *et al.* Peroxisomes protect lymphoma cells from HDAC inhibitor-mediated apoptosis. *Cell Death Differ* 2017;**24**(11):1912-24 doi 10.1038/cdd.2017.115.
24. Pettersson F, Del Rincon SV, Emond A, Huor B, Ngan E, Ng J, *et al.* Genetic and pharmacologic inhibition of eIF4E reduces breast cancer cell migration, invasion, and metastasis. *Cancer Res* 2015;**75**(6):1102-12 doi 10.1158/0008-5472.CAN-14-1996.
25. Yang W, Khoury E, Guo Q, Prabhu SA, Emond A, Huang F, *et al.* MNK1 signaling induces an ANGPTL4-mediated gene signature to drive melanoma progression. *Oncogene* 2020 doi 10.1038/s41388-020-1240-5.
26. Yan HH, Pickup M, Pang Y, Gorska AE, Li Z, Chytil A, *et al.* Gr-1+CD11b+ myeloid cells tip the balance of immune protection to tumor promotion in the premetastatic lung. *Cancer Res* 2010;**70**(15):6139-49 doi 10.1158/0008-5472.CAN-10-0706.
27. Chapman RS, Lourenco PC, Tonner E, Flint DJ, Selbert S, Takeda K, *et al.* Suppression of epithelial apoptosis and delayed mammary gland involution in mice with a conditional knockout of Stat3. *Genes Dev* 1999;**13**(19):2604-16 doi 10.1101/gad.13.19.2604.
28. Wang C, Chen Z, Bu X, Han Y, Shan S, Ren T, *et al.* IL-33 signaling fuels outgrowth and metastasis of human lung cancer. *Biochem Biophys Res Commun* 2016;**479**(3):461-8 doi 10.1016/j.bbrc.2016.09.081.

29. Fang M, Li Y, Huang K, Qi S, Zhang J, Zgodzinski W, *et al.* IL33 Promotes Colon Cancer Cell Stemness via JNK Activation and Macrophage Recruitment. *Cancer Res* 2017;**77**(10):2735-45 doi 10.1158/0008-5472.CAN-16-1602.
30. Li Y, Shi J, Qi S, Zhang J, Peng D, Chen Z, *et al.* IL-33 facilitates proliferation of colorectal cancer dependent on COX2/PGE2. *J Exp Clin Cancer Res* 2018;**37**(1):196 doi 10.1186/s13046-018-0839-7.
31. Shani O, Vorobyov T, Monteran L, Lavie D, Cohen N, Raz Y, *et al.* Fibroblast-Derived IL33 Facilitates Breast Cancer Metastasis by Modifying the Immune Microenvironment and Driving Type 2 Immunity. *Cancer Res* 2020;**80**(23):5317-29 doi 10.1158/0008-5472.CAN-20-2116.
32. Guo Q, Minnier J, Burchard J, Chiotti K, Spellman P, Schedin P. Physiologically activated mammary fibroblasts promote postpartum mammary cancer. *JCI Insight* 2017;**2**(6):e89206 doi 10.1172/jci.insight.89206.
33. Yu XX, Hu Z, Shen X, Dong LY, Zhou WZ, Hu WH. IL-33 Promotes Gastric Cancer Cell Invasion and Migration Via ST2-ERK1/2 Pathway. *Dig Dis Sci* 2015;**60**(5):1265-72 doi 10.1007/s10620-014-3463-1.
34. Zhan Y, Guo J, Yang W, Goncalves C, Rzymski T, Dreas A, *et al.* MNK1/2 inhibition limits oncogenicity and metastasis of KIT-mutant melanoma. *J Clin Invest* 2017;**127**(11):4179-92 doi 10.1172/JCI91258.
35. Quail DF, Olson OC, Bhardwaj P, Walsh LA, Akkari L, Quick ML, *et al.* Obesity alters the lung myeloid cell landscape to enhance breast cancer metastasis through IL5 and GM-CSF. *Nat Cell Biol* 2017;**19**(8):974-87 doi 10.1038/ncb3578.
36. Zaynagetdinov R, Sherrill TP, Gleaves LA, McLoed AG, Saxon JA, Habermann AC, *et al.* Interleukin-5 facilitates lung metastasis by modulating the immune microenvironment. *Cancer Res* 2015;**75**(8):1624-34 doi 10.1158/0008-5472.CAN-14-2379.
37. Papageorgis P, Ozturk S, Lambert AW, Neophytou CM, Tzatsos A, Wong CK, *et al.* Targeting IL13Ralpha2 activates STAT6-TP63 pathway to suppress breast cancer lung metastasis. *Breast Cancer Res* 2015;**17**:98 doi 10.1186/s13058-015-0607-y.
38. Olkhanud PB, Baatar D, Bodogai M, Hakim F, Gress R, Anderson RL, *et al.* Breast cancer lung metastasis requires expression of chemokine receptor CCR4 and regulatory T cells. *Cancer Res* 2009;**69**(14):5996-6004 doi 10.1158/0008-5472.CAN-08-4619.
39. Berlato C, Khan MN, Schioppa T, Thompson R, Maniati E, Montfort A, *et al.* A CCR4 antagonist reverses the tumor-promoting microenvironment of renal cancer. *J Clin Invest* 2017;**127**(3):801-13 doi 10.1172/JCI82976.
40. Brenot A, Knolhoff BL, DeNardo DG, Longmore GD. SNAIL1 action in tumor cells influences macrophage polarization and metastasis in breast cancer through altered GM-CSF secretion. *Oncogenesis* 2018;**7**(3):32 doi 10.1038/s41389-018-0042-x.
41. Chen L, Wang S, Wang Y, Zhang W, Ma K, Hu C, *et al.* IL-6 influences the polarization of macrophages and the formation and growth of colorectal tumor. *Oncotarget* 2018;**9**(25):17443-54 doi 10.18632/oncotarget.24734.
42. Duluc D, Delneste Y, Tan F, Moles MP, Grimaud L, Lenoir J, *et al.* Tumor-associated leukemia inhibitory factor and IL-6 skew monocyte differentiation into tumor-associated macrophage-like cells. *Blood* 2007;**110**(13):4319-30 doi 10.1182/blood-2007-02-072587.
43. Miyake M, Hori S, Morizawa Y, Tatsumi Y, Nakai Y, Anai S, *et al.* CXCL1-Mediated Interaction of Cancer Cells with Tumor-Associated Macrophages and Cancer-Associated

Fibroblasts Promotes Tumor Progression in Human Bladder Cancer. *Neoplasia* 2016;**18**(10):636-46 doi 10.1016/j.neo.2016.08.002.

44. Mondini M, Loyher PL, Hamon P, Gerbe de Thore M, Laviron M, Berthelot K, *et al.* CCR2-Dependent Recruitment of Tregs and Monocytes Following Radiotherapy Is Associated with TNFalpha-Mediated Resistance. *Cancer Immunol Res* 2019;**7**(3):376-87 doi 10.1158/2326-6066.CIR-18-0633.
45. Wang D, Sun H, Wei J, Cen B, DuBois RN. CXCL1 Is Critical for Premetastatic Niche Formation and Metastasis in Colorectal Cancer. *Cancer Res* 2017;**77**(13):3655-65 doi 10.1158/0008-5472.CAN-16-3199.
46. Weber R, Fleming V, Hu X, Nagibin V, Groth C, Altevogt P, *et al.* Myeloid-Derived Suppressor Cells Hinder the Anti-Cancer Activity of Immune Checkpoint Inhibitors. *Front Immunol* 2018;**9**:1310 doi 10.3389/fimmu.2018.01310.
47. Zhu H, Gu Y, Xue Y, Yuan M, Cao X, Liu Q. CXCR2(+) MDSCs promote breast cancer progression by inducing EMT and activated T cell exhaustion. *Oncotarget* 2017;**8**(70):114554-67 doi 10.18632/oncotarget.23020.
48. Wherry EJ. T cell exhaustion. *Nat Immunol* 2011;**12**(6):492-9.
49. Tassi E, Grazia G, Vegetti C, Bersani I, Bertolini G, Molla A, *et al.* Early Effector T Lymphocytes Coexpress Multiple Inhibitory Receptors in Primary Non-Small Cell Lung Cancer. *Cancer Res* 2017;**77**(4):851-61 doi 10.1158/0008-5472.CAN-16-1387.
50. Zhan Y, Guo J, Yang W, Goncalves C, Rzymski T, Dreas A, *et al.* MNK1/2 inhibition limits oncogenicity and metastasis of KIT-mutant melanoma. *J Clin Invest* 2017 doi 10.1172/JCI91258.
51. Callihan EB, Gao D, Jindal S, Lyons TR, Manthey E, Edgerton S, *et al.* Postpartum diagnosis demonstrates a high risk for metastasis and merits an expanded definition of pregnancy-associated breast cancer. *Breast cancer research and treatment* 2013;**138**(2):549-59 doi 10.1007/s10549-013-2437-x.
52. Johansson AL, Andersson TM, Hsieh CC, Cnattingius S, Lambe M. Increased mortality in women with breast cancer detected during pregnancy and different periods postpartum. *Cancer Epidemiol Biomarkers Prev* 2011;**20**(9):1865-72 doi 10.1158/1055-9965.EPI-11-0515.
53. Fournie JJ, Poupot M. The Pro-tumorigenic IL-33 Involved in Antitumor Immunity: A Yin and Yang Cytokine. *Front Immunol* 2018;**9**:2506 doi 10.3389/fimmu.2018.02506.
54. Molofsky AB, Savage AK, Locksley RM. Interleukin-33 in Tissue Homeostasis, Injury, and Inflammation. *Immunity* 2015;**42**(6):1005-19 doi 10.1016/j.immuni.2015.06.006.
55. Duerr CU, Fritz JH. Regulation of group 2 innate lymphoid cells. *Cytokine* 2016;**87**:1-8 doi 10.1016/j.cyto.2016.01.018.
56. Li J, Razumilava N, Gores GJ, Walters S, Mizuochi T, Mourya R, *et al.* Biliary repair and carcinogenesis are mediated by IL-33-dependent cholangiocyte proliferation. *J Clin Invest* 2014;**124**(7):3241-51 doi 10.1172/JCI73742.
57. Moral JA, Leung J, Rojas LA, Ruan J, Zhao J, Sethna Z, *et al.* ILC2s amplify PD-1 blockade by activating tissue-specific cancer immunity. *Nature* 2020;**579**(7797):130-5 doi 10.1038/s41586-020-2015-4.
58. Acharyya S, Oskarsson T, Vanharanta S, Malladi S, Kim J, Morris PG, *et al.* A CXCL1 paracrine network links cancer chemoresistance and metastasis. *Cell* 2012;**150**(1):165-78 doi 10.1016/j.cell.2012.04.042.

59. Salgado R, Junius S, Benoy I, Van Dam P, Vermeulen P, Van Marck E, *et al.* Circulating interleukin-6 predicts survival in patients with metastatic breast cancer. *Int J Cancer* 2003;**103**(5):642-6 doi 10.1002/ijc.10833.
60. Lu DP, Zhou XY, Yao LT, Liu CG, Ma W, Jin F, *et al.* Serum soluble ST2 is associated with ER-positive breast cancer. *BMC cancer* 2014;**14**:198 doi 10.1186/1471-2407-14-198.
61. Yang ZP, Ling DY, Xie YH, Wu WX, Li JR, Jiang J, *et al.* The Association of Serum IL-33 and sST2 with Breast Cancer. *Dis Markers* 2015;**2015**:516895 doi 10.1155/2015/516895.
62. Sharma P, Allison JP. The future of immune checkpoint therapy. *Science (New York, NY)* 2015;**348**(6230):56-61 doi 10.1126/science.aaa8172.
63. Tamburini BAJ, Elder AM, Finlon JM, Winter AB, Wessells VM, Borges VF, *et al.* PD-1 Blockade During Post-partum Involution Reactivates the Anti-tumor Response and Reduces Lymphatic Vessel Density. *Front Immunol* 2019;**10**:1313 doi 10.3389/fimmu.2019.01313.
64. Xu Y, Poggio M, Jin HY, Shi Z, Forester CM, Wang Y, *et al.* Translation control of the immune checkpoint in cancer and its therapeutic targeting. *Nature medicine* 2019;**25**(2):301-11 doi 10.1038/s41591-018-0321-2.

Figure legends

Figure 1. Stromal phospho-eIF4E deficiency (eIF4E^{S209A}) protects against lung metastasis in a pre-clinical model of post-partum breast cancer (PPBC) and alters the immune landscape at the lung metastatic site.

A. Timeline of the PPBC mouse model. Weeks refer to the approximate age of mice, see methods for further details. **B.** 66cl4 cells injected into the involuting mammary gland grow at a similar rate in WT and eIF4E^{S209A} PPBC mice. Data are presented as mean tumor volume ±SEM at each time point. **C.** Fewer lung metastases are present in eIF4E^{S209A} 66cl4 PPBC mice, compared to WT PPBC mice. Data are presented as average tumor burden in the lung (scale bar=4mm). Data in (**1B-C**) are pooled from two independent biological experiments (WT n=12, eIF4E^{S209A} n=17) **D.** Blood from eIF4E^{S209A} 66cl4 tumor-bearing PPBC animals at day 14 of tumor growth contains fewer circulating tumor cells compared to WT. Data are presented as sum of tumor cells counted in 4 fields of view at 10x magnification using a brightfield microscope after 7 days of culture in 6-thioguanine selection media. Each dot represents an individual mouse (WT n=10, S209A n=9), data are pooled from two independent biological experiments. **E.** The numbers of Ki67^{+} cells in the lung metastases are similar between the WT and eIF4E^{S209A} BALB/c 66cl4 PPBC mice. Data are presented as % Ki67^{+} cells per lung, each dot represents individual animals (scale bar=200μm, WT n=9, eIF4E^{S209A} n=12) and are pooled from two independent biological experiments. **F.** E0771 primary PPBC tumors grow at a similar rate in WT and eIF4E^{S209A} C57BL/6N E0771 PPBC animals. Data are presented as mean tumor volume ±SEM at each time point **G.** E0771 PPBC eIF4E^{S209A} hosts (C57BL/6N) have fewer metastases than in WT PPBC animals. Data are presented as average tumor burden in the lung, each dot represents an individual mouse. Data in **(1F-G)** are pooled from two independent biological

experiments (WT n=8, eIF4E^{S209A} n=13). **H.** Immune phenotyping by multicolor flow cytometry of the lungs of eIF4E^{S209A} PPBC mice injected with 66cl4 tumor cells during mammary gland involution reveals an increased total number of CD3^{+} T cells and cytotoxic CD8^{+} T cells, as well as a decreased number of CD11b^{+}Ly6G^{+} cells at 33 days post tumor cell injection. Each dot represents an individual mouse, (WT n=5, eIF4E^{S209A} n=8), data are pooled from two independent biological experiments. In panels (**1C-E), (1G-H)**, the horizontal bar indicates the mean of the cohort, error bars indicate SEM. Two-tailed Mann-Whitney test (**1C-D, 1G-H**), unpaired t-test (**1E**) or two way ANOVA (**1B, 1F**) was used to calculate statistical significance.

Figure 2. Phospho-eIF4E-deficient fibroblasts secrete less IL-33 and repress tumor cell invasion in co-culture assays.

A. 66cl4 PPBC tumors grown in WT BALB/c hosts express more IL-33, than the same tumors grown in phospho-eIF4E-deficient ($eIF4E^{S209A}$) hosts. Each dot represents individual animals, the horizontal bar indicates the mean of the cohort, error bars indicate SEM (scale bar=40μm, WT n=11, $eIF4E^{S209A}$ n=9). **B**. The correlation between the expression of phospho-eIF4E (referred to as p-eIF4E in the figures henceforth) and IL-33 in 9 PPBC tumors was assessed by calculating Spearman correlation coefficient. A representative image showing IL-33 and p-eIF4E expression (Scale bar=50μm). **C.** Membrane-based cytokine array profiling of the conditioned media from WT and $eIF4E^{S200A}$ primary mammary gland fibroblasts. Shown is the expression of IL-33 detected in the conditioned media from one representative pool of cells per condition, each pool comprising 3 individual animals. **D.** Cultured primary mammary gland $eIF4E^{S209A}$ fibroblasts secrete less IL-33 than WT mammary fibroblasts. Data represent two separate pools of fibroblasts per condition (different from data shown in **2C**), each pool originating from three animals and are presented as mean ±SD. **E.** $eIF4E^{S209A}$ mouse embryonic fibroblasts express less IL-33. One representative Western blot out of three independent experiments is shown. **F.** Schematic overview of the mouse embryonic fibroblast (MEF)-tumor cell co-culture experiments used to generate data in panels **3G-M**. **G.** 66cl4 cells invade less in the presence of $eIF4E^{S209A}$ fibroblasts, compared to co-culturing with WT fibroblasts. Bars represent the percentage of 66cl4 cells invaded, compared to 66cl4 co-cultured with WT fibroblasts. A summary of three biological replicates +SD is shown. **H.** $eIF4E^{S209A}$ fibroblasts express less *Il33* mRNA after co-culture with 66cl4 cells. Data represent three biological replicates normalized to housekeeping gene *Rplp0* and are presented as mean +SD. **I.** $eIF4E^{S209A}$ fibroblasts express less IL-33 protein

compared to WT fibroblasts, IL-33 expression is induced in WT, but not eIF4E^{S209A} fibroblasts when 66cl4 cancer cells are present. One representative experiment out of three biological replicates is shown. **J.** SEL201 inhibits IL-33 protein expression in WT fibroblasts when co-cultured with 66cl4 cells. One representative experiment out of three biological replicates is shown. **K.** SEL201-treatment of WT fibroblasts suppresses 66cl4 invasion, when co-cultured. Bars represent the percentage of 66cl4 cells invaded compared to 66cl4 co-cultured with WT fibroblasts in absence of SEL201 and a summary of three biological replicates +SD is shown. **L.** SEL201 treatment decreases IL-33 and p-eIF4E protein levels in patient-derived CAFs. **M.** MDA-MB-231 breast cancer cell invasion is repressed when co-cultured with SEL201-treated patient-derived CAFs. Data represent one experiment per donor. Every dot represents number of cells invaded per field of image, the horizontal bar and error bars show mean of the group and SD respectively (representative images shown). Unpaired t-test (**2A, 2D, 2H, 2K**), multiple comparison one way ANOVA (**2G**) or two way ANOVA (**2M**) was used to calculate statistical significance.

Figure 3. Recombinant IL-33 induces tumor cell invasion and upregulates the expression of immune suppressive chemokines and cytokines.

A. Knockdown of *Il1rl1* (encodes ST2) in 66cl4 cells diminishes their invasion toward fibroblasts. Bars represent the number of cells invaded per field of image (representative images shown) and a summary of three biological replicates is shown. **B.** 50ng/ml rIL-33 treatment for 6h induces the phosphorylation of p38 and eIF4E in 66cl4 cells. One representative experiment out of three is shown. **C.** rIL-33 enhances 66cl4 cell invasion. Bars represent the number of cells invaded per field of image and a summary of three biological replicates +SD is shown. **D.** rIL-33 induces the expression of *Cxcl1, Ccl17, Csf2,* and *Il6* mRNA in 66cl4 cells. rIL-33 does not induce the mRNA expression of *Il4* and *Cxcl2* in 66cl4 cells. Data represent three biological replicates and are presented as mean +SD. **E.** SEL201 treatment reduces IL-13 and IL-5 secretion of WT ILC2s. **F.** SEL201 does not impact the proliferation of WT ILC2s. Panels **(3E-F)**, ILC2 cells were isolated from the bone marrow of BALB/c mice and *ex vivo* expanded. Data represent two biological replicates, each comprising 3 technical replicates and are presented as mean +SD. Multiple comparison one way ANOVA (**3A**), unpaired t-test (**3C-D**), or two way ANOVA (**3E-F**) was used to calculate statistical significance.

Figure 4. Imaging of the human PPBC TME.

A. Positive correlation between IL-33 protein expression in human PPBC samples (n=9) and p-eIF4E levels. Spearman correlation was used to calculate statistical significance. **B.** Spearman correlation analysis of the mRNA expression of *MKNK1* (encodes MNK1) and *IL33* using the TCGA breast cancer database (1217 samples). **C.** Imaging mass cytometry (one image shown, left) revealed the proportion of different cell types, and their level of phospho-eIF4E expression, in 8 human nulliparous breast tumors (BC), 6 pregnancy associated breast cancers (PrBC), and 9 postpartum breast cancers (PPBC). Each dot represents one cell. **D.** Phospho-eIF4E and PD-L1 expression are detected in human tumor cells. Percentage of positive cells (defined by the grey dashed bar) are shown atop of each group. Each dot represents one cell. **E.** PPBC samples have increased $CD8^+$ T cell infiltration, compared to BC and PrBC samples. Percentage of positive cells (defined by the grey dashed bar) are shown atop of each group. Each dot represents the proportion of cell per core. **F.** $CD8^+$ T cells in PPBC have increased surface expression of HLA-DR and PD-1, compared to BC and PrBC. Percentage of positive cells (defined by the grey dashed bar) are shown atop of each group. Each dot represents one cell. Expression of $CD8^+$HLA-DR^+ T cells and $CD8^+$PD-1^+ T cells correlate in each individual PPBC core. Each dot represents the proportion of cell per core. Spearman correlation was used to calculate statistical significance. **G.** Tumor-infiltrating T cells in tumors grown in WT and $eIF4E^{S209A}$ mice show differences in the expression of activation markers IFNγ (left panel) and CD107a (right panel). Each dot represents an individual mouse (WT n=11, S209A n=9) pooled from two independent biological experiments, horizontal bar and error bars represent the mean of the cohort and SEM respectively. Multiple comparison one way ANOVA (**4C-F**) or unpaired t-test (**4G)** was used to calculate statistical significance.

Figure 5. Sensitization of murine PPBC to PD-1 blockade using a MNK1/2 inhibitor
A. Lungs of tumor-bearing S209A animals show higher frequency of $CD8^+$ cells at day 14 of tumor development compared to lungs of WT animals**. B.** Higher frequency of $CD8^+$ cells recruited to lungs of S209A tumor-bearing animals express the activation marker IFNγ compared to WT. Each dot in **(A,B)** represents an individual mouse (WT n=11, S209A n=9) pooled from two independent biological experiments, horizontal bar and error bars represent the mean of the cohort and SEM respectively. **C.** SEL201 administered alone or in combination with anti-PD-1 blockade does not significantly alter primary tumor outgrowth. Data are presented as mean tumor volume ±SEM at each time point. Vehicle group n=5, anti-PD-1 treated group n=4, SEL201-treated group n=5, SEL201+anti-PD-1 group n= 5, one representative tumor growth curve out of two independent biological experiments is shown. **D.** Combination of SEL201 plus anti-PD-1 significantly decreased 66cl4 lung metastatic burden in the PPBC model. Data are presented as average tumor burden in the lung (representative images of the lung metastases are shown), each dot represents an individual animal and the horizontal bar and error bars indicate the mean of the cohort and SEM respectively. Scale bar=4mm. Vehicle group n=10, anti-PD-1 treated group n=8, SEL201-treated group n=12, SEL201+anti-PD-1 group n=10. **E.** SEL201 treatment efficiently repressed phospho-eIF4E expression and significantly increased the number of $CD8^+$ T cells in the lung metastases (shown by IHC). White arrows on the representative images indicate $CD8^+$ T cells. Scale bar=50μm. Each dot in the graphs represents one animal and the horizontal bar and error bars indicate the mean of the cohort and SEM respectively. Vehicle group n=7, anti-PD-1 treated group n=5, SEL201-treated group n=7, SEL201+anti-PD-1 group n=7. Data in (**5C-E**) are pooled from two independent biological experiments. Unpaired t-test (**5A-B**), multiple comparison one way ANOVA (**5D-E**) or two way ANOVA (**5C**) was used to calculate statistical significance.

Figure 1

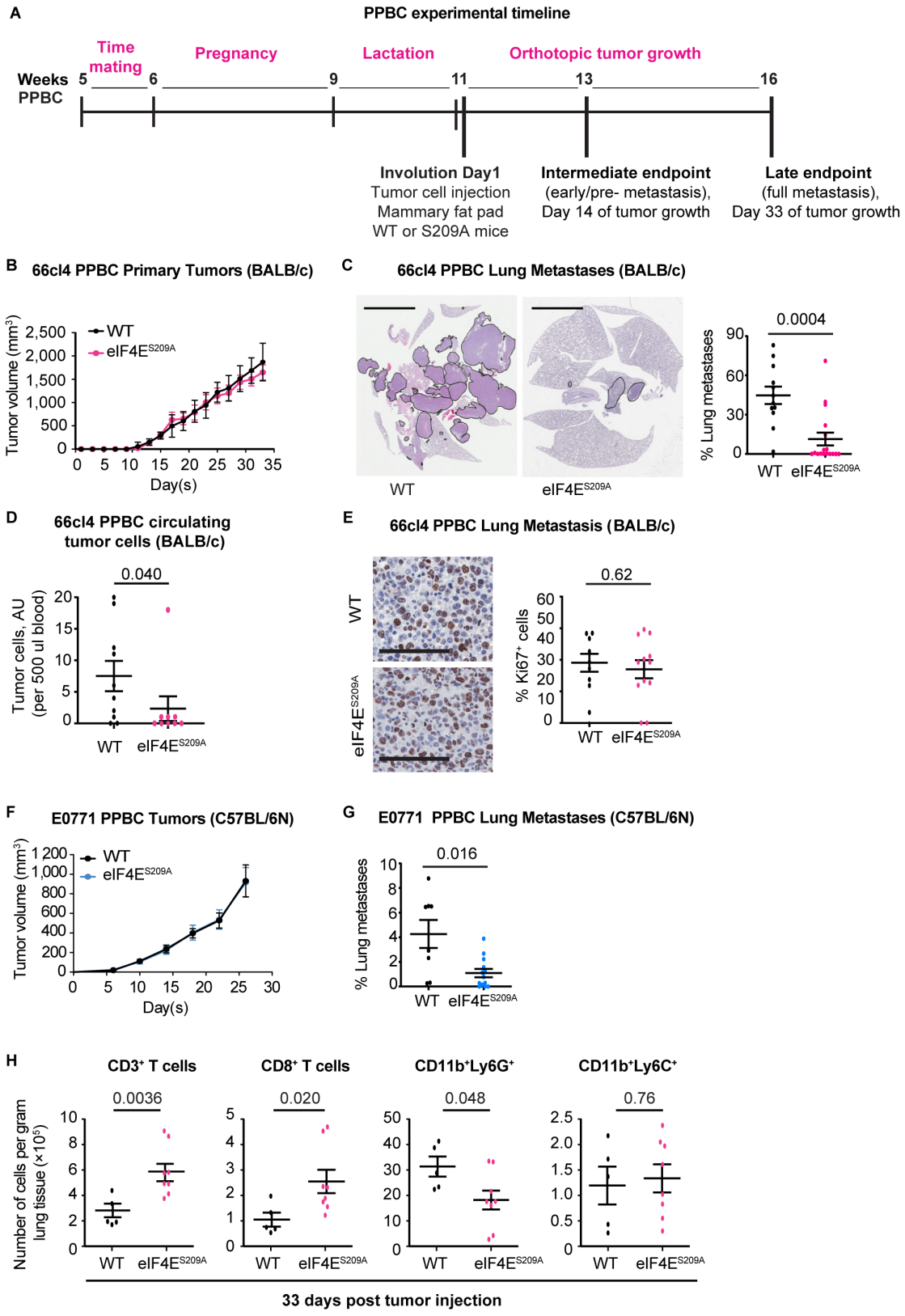
A
PPBC experimental timeline
Time mating
Pregnancy
Lactation
Orthotopic tumor growth
Weeks PPBC
5
6
9
11
13
16
Involution Day1
Tumor cell injection
Mammary fat pad
WT or S209A mice
Intermediate endpoint
(early/pre- metastasis),
Day 14 of tumor growth
Late endpoint
(full metastasis),
Day 33 of tumor growth
B
66cl4 PPBC Primary Tumors (BALB/c)
Tumor volume (mm3)
WT
eIF4ES209A
Day(s)
C
66cl4 PPBC Lung Metastases (BALB/c)
WT
eIF4ES209A
% Lung metastases
0.0004
D
66cl4 PPBC circulating tumor cells (BALB/c)
Tumor cells, AU (per 500 ul blood)
0.040
E
66cl4 PPBC Lung Metastasis (BALB/c)
% Ki67+ cells
0.62
F
E0771 PPBC Tumors (C57BL/6N)
G
E0771 PPBC Lung Metastases (C57BL/6N)
0.016
H
CD3+ T cells
CD8+ T cells
CD11b+Ly6G+
CD11b+Ly6C+
Number of cells per gram lung tissue (×10^5)
0.0036
0.020
0.048
0.76
33 days post tumor injection

Figure 2

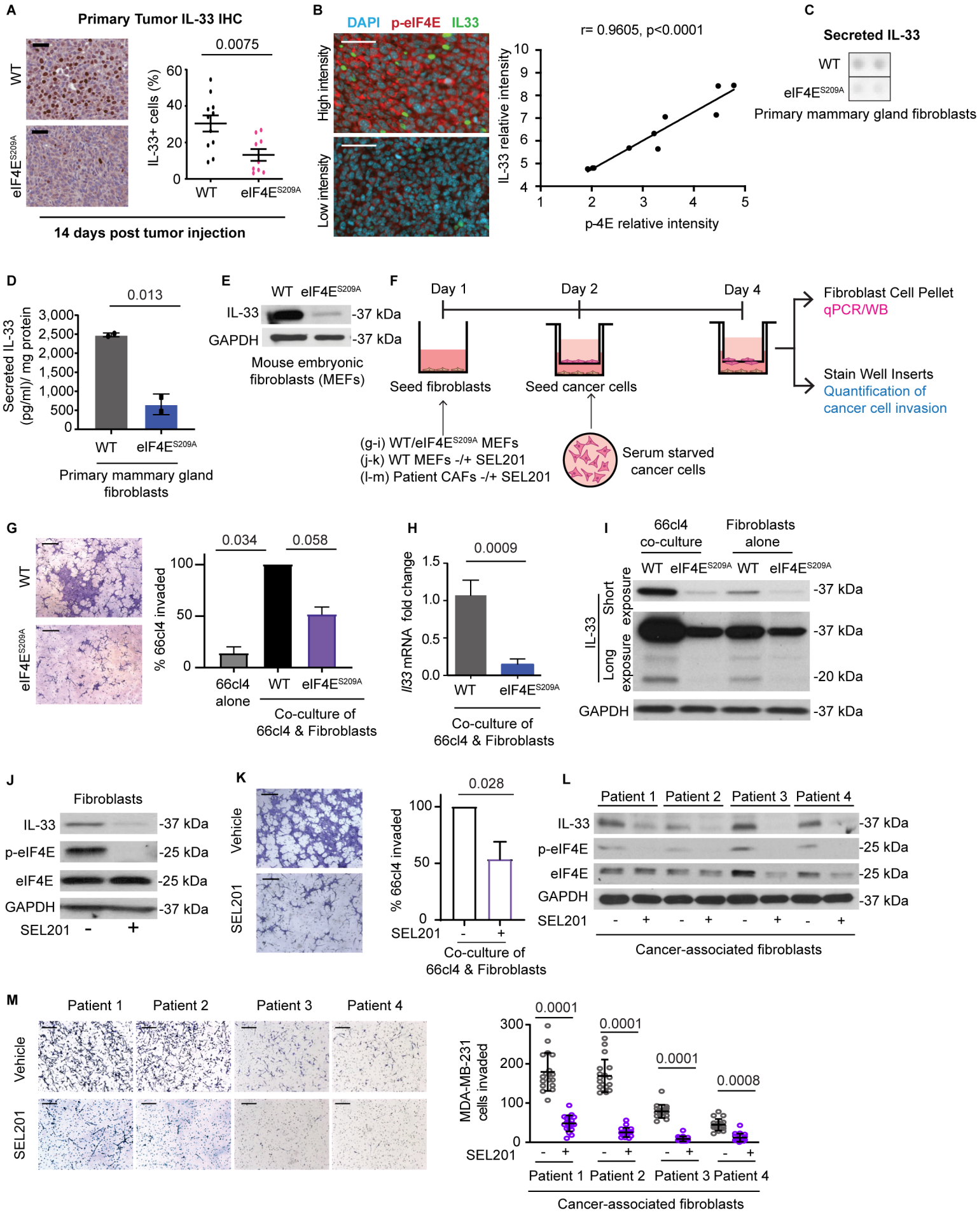
A
Primary Tumor IL-33 IHC
WT
eIF4E S209A
0.0075
IL-33+ cells (%)
60
40
20
0
WT
eIF4E S209A
14 days post tumor injection
B
DAPI p-eIF4E IL33
High intensity
Low intensity
r= 0.9605, p<0.0001
IL-33 relative intensity
p-4E relative intensity
C
Secreted IL-33
WT
eIF4E S209A
Primary mammary gland fibroblasts
D
0.013
Secreted IL-33 (pg/ml)/ mg protein
3,000
2,500
2,000
1,500
1,000
500
0
WT
eIF4E S209A
Primary mammary gland fibroblasts
E
WT eIF4E S209A
IL-33
-37 kDa
GAPDH
-37 kDa
Mouse embryonic fibroblasts (MEFs)
F
Day 1
Day 2
Day 4
Fibroblast Cell Pellet
qPCR/WB
Stain Well Inserts
Quantification of cancer cell invasion
Seed fibroblasts
Seed cancer cells
(g-i) WT/eIF4E S209A MEFs
(j-k) WT MEFs -/+ SEL201
(l-m) Patient CAFs -/+ SEL201
Serum starved cancer cells
G
WT
eIF4E S209A
0.034
0.058
% 66cl4 invaded
100
50
0
66cl4 alone
WT
eIF4E S209A
Co-culture of 66cl4 & Fibroblasts
H
0.0009
Il33 mRNA fold change
1.5
1.0
0.5
0.0
WT
eIF4E S209A
Co-culture of 66cl4 & Fibroblasts
I
66cl4 co-culture
Fibroblasts alone
WT eIF4E S209A WT eIF4E S209A
IL-33
Short exposure
Long exposure
-37 kDa
-37 kDa
-20 kDa
GAPDH
-37 kDa
J
Fibroblasts
IL-33
-37 kDa
p-eIF4E
-25 kDa
eIF4E
-25 kDa
GAPDH
-37 kDa
SEL201 - +
K
Vehicle
SEL201
0.028
% 66cl4 invaded
100
50
0
SEL201 - +
Co-culture of 66cl4 & Fibroblasts
L
Patient 1 Patient 2 Patient 3 Patient 4
IL-33
p-eIF4E
eIF4E
GAPDH
SEL201
-37 kDa
-25 kDa
-25 kDa
-37 kDa
- + - + - + - +
Cancer-associated fibroblasts
M
Patient 1 Patient 2 Patient 3 Patient 4
Vehicle
SEL201
0.0001
0.0001
0.0001
0.0008
MDA-MB-231 cells invaded
300
200
100
0
SEL201 - + - + - + - +
Patient 1 Patient 2 Patient 3 Patient 4
Cancer-associated fibroblasts

Figure 3

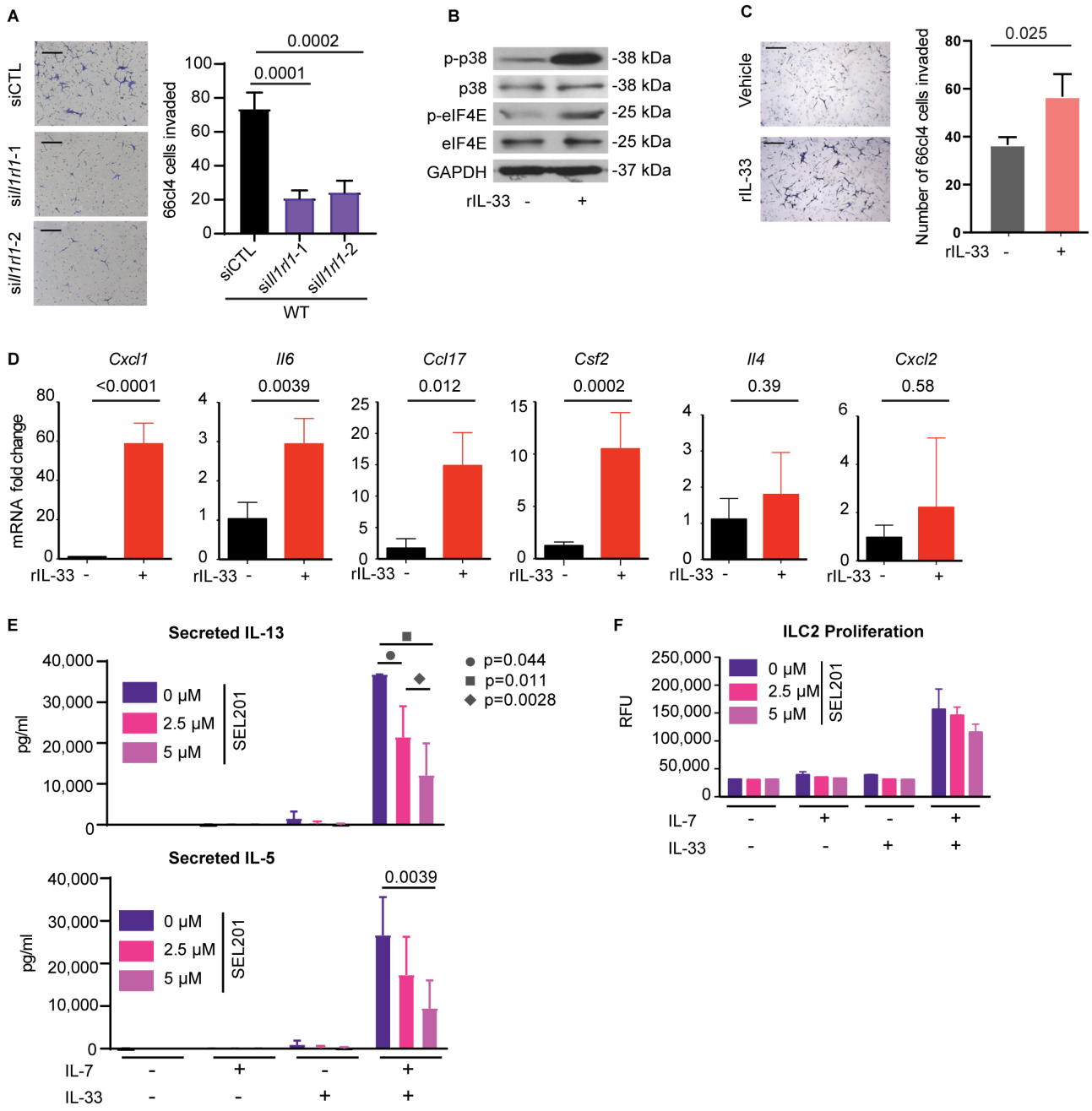
A
siCTL
sil1rl1-1
sil1rl1-2
66cl4 cells invaded
0.0002
0.0001
siCTL
sil1rl1-1
sil1rl1-2
WT
B
p-p38
p38
p-eIF4E
eIF4E
GAPDH
-38 kDa
-38 kDa
-25 kDa
-25 kDa
-37 kDa
rIL-33 - +
C
Vehicle
rIL-33
Number of 66cl4 cells invaded
0.025
rIL-33 - +
D
Cxcl1
<0.0001
Il6
0.0039
Ccl17
0.012
Csf2
0.0002
Il4
0.39
Cxcl2
0.58
mRNA fold change
rIL-33 - +
E
Secreted IL-13
pg/ml
0 µM
2.5 µM
5 µM
SEL201
p=0.044
p=0.011
p=0.0028
Secreted IL-5
0.0039
IL-7
IL-33
F
ILC2 Proliferation
RFU
0 µM
2.5 µM
5 µM
SEL201
IL-7
IL-33

Figure 4

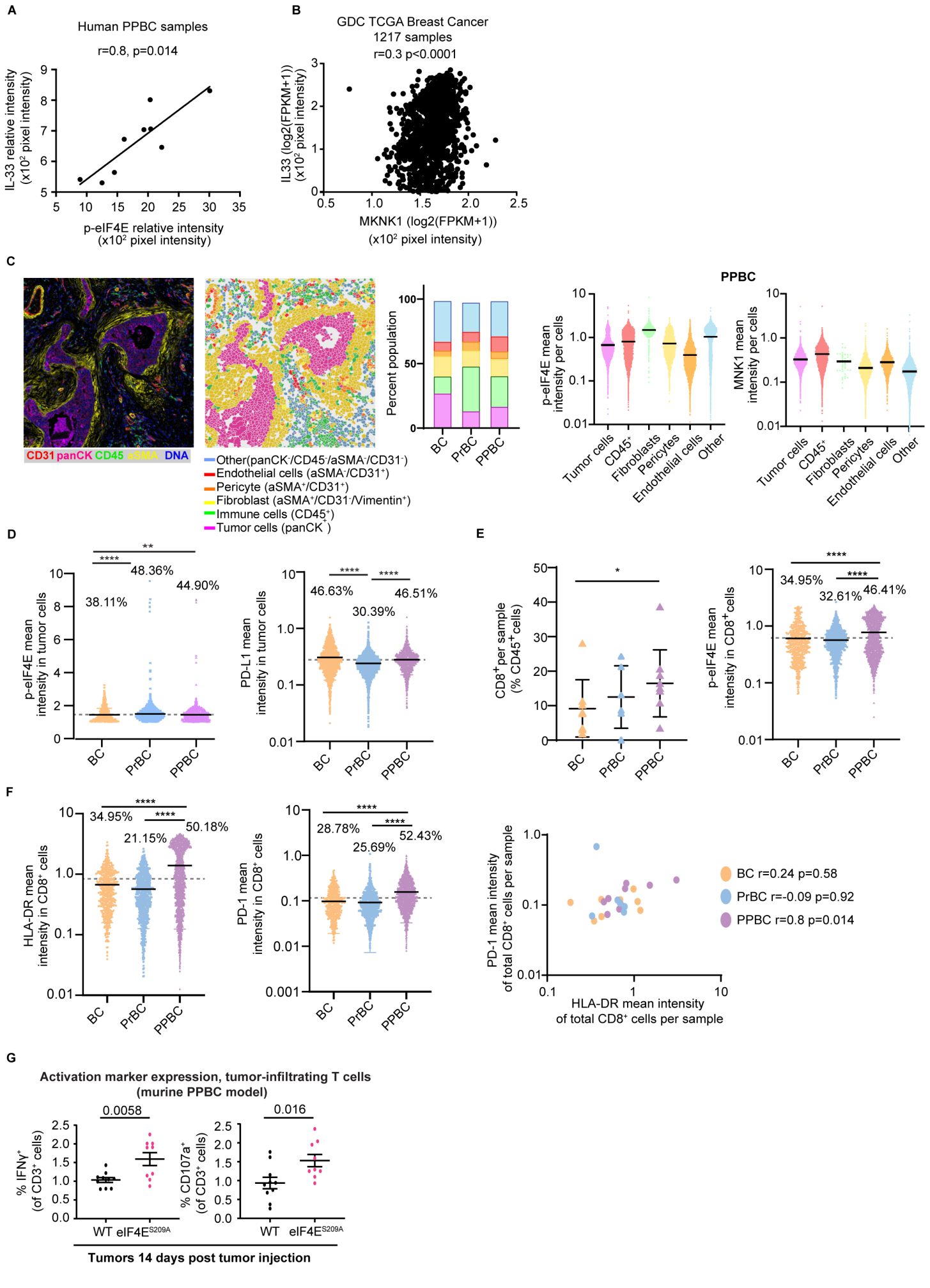
A
Human PPBC samples
r=0.8, p=0.014
IL-33 relative intensity (x10² pixel intensity)
p-eIF4E relative intensity (x10² pixel intensity)
B
GDC TCGA Breast Cancer
1217 samples
r=0.3 p<0.0001
IL33 (log2(FPKM+1)) (x10² pixel intensity)
MKNK1 (log2(FPKM+1)) (x10² pixel intensity)
C
CD31 panCK CD45 aSMA DNA
Other(panCK-/CD45-/aSMA-/CD31-)
Endothelial cells (aSMA-/CD31+)
Pericyte (aSMA+/CD31+)
Fibroblast (aSMA+/CD31-/Vimentin+)
Immune cells (CD45+)
Tumor cells (panCK+)
Percent population
BC
PrBC
PPBC
PPBC
p-eIF4E mean intensity per cells
MNK1 mean intensity per cells
Tumor cells
CD45+
Fibroblasts
Pericytes
Endothelial cells
Other
D
p-eIF4E mean intensity in tumor cells
38.11%
48.36%
44.90%
PD-L1 mean intensity in tumor cells
46.63%
30.39%
46.51%
E
CD8+ per sample (% CD45+ cells)
p-eIF4E mean intensity in CD8+ cells
34.95%
32.61%
46.41%
F
HLA-DR mean intensity in CD8+ cells
34.95%
21.15%
50.18%
PD-1 mean intensity in CD8+ cells
28.78%
25.69%
52.43%
PD-1 mean intensity of total CD8+ cells per sample
HLA-DR mean intensity of total CD8+ cells per sample
BC r=0.24 p=0.58
PrBC r=-0.09 p=0.92
PPBC r=0.8 p=0.014
G
Activation marker expression, tumor-infiltrating T cells (murine PPBC model)
0.0058
0.016
% IFNγ+ (of CD3+ cells)
% CD107a+ (of CD3+ cells)
WT
eIF4E S209A
Tumors 14 days post tumor injection

Figure 5

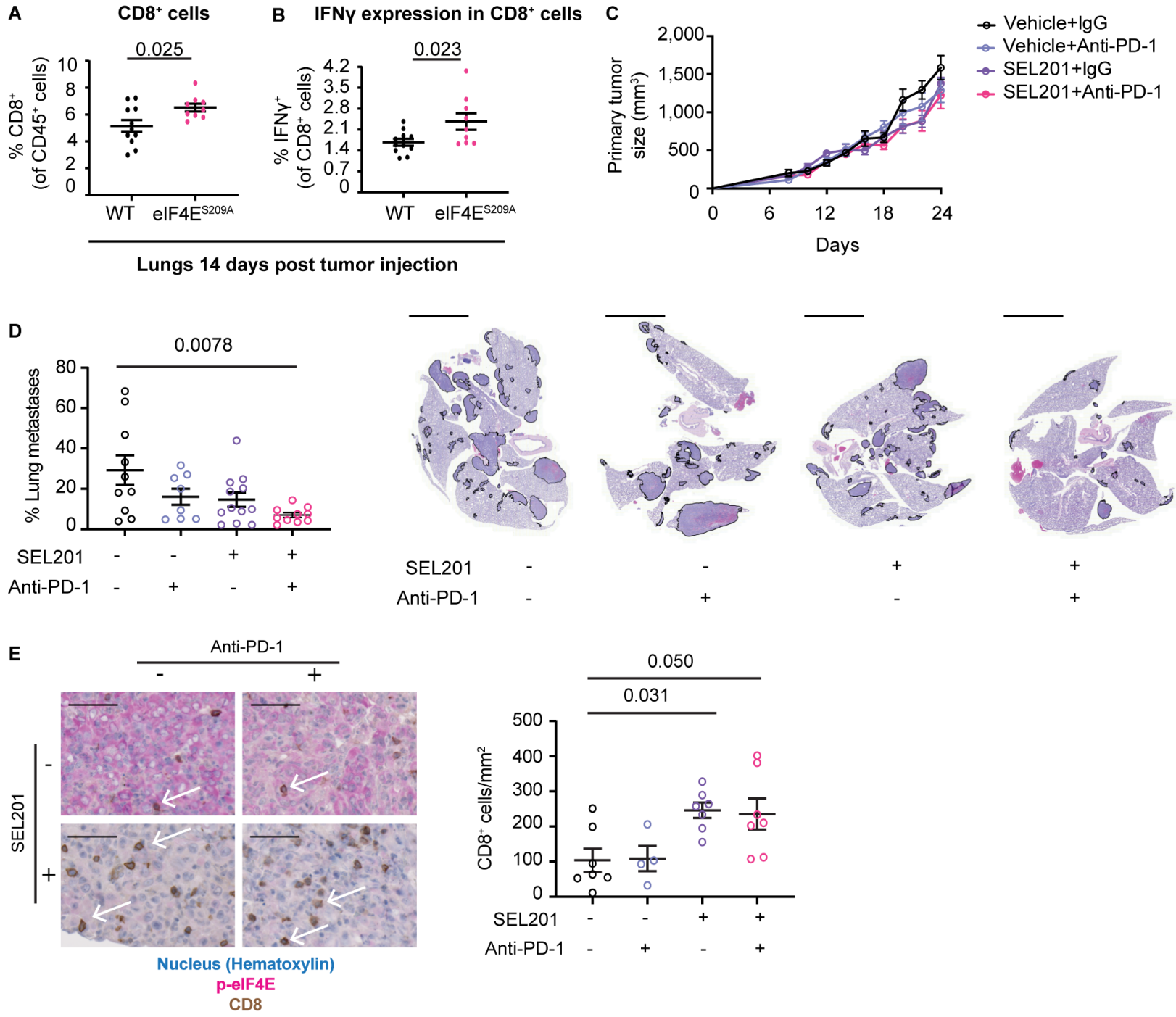
A
CD8⁺ cells
0.025
% CD8⁺ (of CD45⁺ cells)
WT
eIF4E^S209A
B
IFNγ expression in CD8⁺ cells
0.023
% IFNγ⁺ (of CD8⁺ cells)
WT
eIF4E^S209A
Lungs 14 days post tumor injection
C
Vehicle+IgG
Vehicle+Anti-PD-1
SEL201+IgG
SEL201+Anti-PD-1
Primary tumor size (mm³)
Days
D
0.0078
% Lung metastases
SEL201
Anti-PD-1
E
Anti-PD-1
SEL201
Nucleus (Hematoxylin)
p-eIF4E
CD8
0.050
0.031
CD8⁺ cells/mm²
SEL201
Anti-PD-1